energies

MDPI

Review

Floating Offshore Vertical Axis Wind Turbines: Opportunities, Challenges and Way Forward

Abel Arredondo-Galeana * and Feargal Brennan

Department of Naval Architecture, Ocean and Marine Engineering, University of Strathclyde, Glasgow G4 0LZ, UK; feargal.brennan@strath.ac.uk
* Correspondence: abel.arredondo-galeana@strath.ac.uk

Abstract: The offshore wind sector is expanding to deep water locations through floating platforms. This poses challenges to horizontal axis wind turbines (HAWTs) due to the ever growing size of blades and floating support structures. As such, maintaining the structural integrity and reducing the levelised cost of energy (LCoE) of floating HAWTs seems increasingly difficult. An alternative to these challenges could be found in floating offshore vertical axis wind turbines (VAWTs). It is known that VAWTs have certain advantages over HAWTs, and in fact, some small-scale developers have successfully commercialised their onshore prototypes. In contrast, it remains unknown whether VAWTs can offer an advantage for deep water floating offshore wind farms. Therefore, here we present a multi-criteria review of different aspects of VAWTs to address this question. It is found that wind farm power density and reliability could be decisive factors to make VAWTs a feasible alternative for deep water floating arrays. Finally, we propose a way forward based on the findings of this review.

Keywords: vertical axis wind turbine; VAWT; floating offshore wind; offshore wind

Citation: Arredondo-Galeana, A.; Brennan, F. Floating Offshore Vertical Axis Wind Turbines: Opportunities, Challenges and Way Forward. *Energies* **2021**, *14*, 8000. https://doi.org/10.3390/en14238000

Academic Editor: Davide Astolfi

Received: 22 October 2021
Accepted: 23 November 2021
Published: 30 November 2021

1. Introduction

Offshore Wind in Northern Europe, North America and Asia has to date become a great success surpassing most commercial and technical expectations [1]. Driven by climate change and governmental subsidies [2], the success of the sector has increased investor confidence and led to ambitious targets, as governments around the world try to achieve zero emissions by 2050. In the UK, for example, early in 2019, a detailed Offshore Wind Sector Deal [3] was committed to 30 GW of electric power with 60% local content by 2030, representing a major component of UK strategic electricity policy. Subsequently, the UK government extended this target to 40 GW by 2030 [4], following the December 2019 national election. In Denmark, tendering for an artificial energy hub island, powered by offshore turbines, is starting in 2022, with a potential capacity of 10 GW by 2030 [5].

Ambitious targets, such as the aforementioned ones, are pushing the horizons of Offshore Wind and the sector is expanding to deep water locations through floating platforms. In the UK, 1 GW of wind power is planned by 2030 from floating offshore wind. Across Europe, a few prototype floating wind farms are already in operation, such as Hywind Scotland and Kincardine Offshore Wind Farm, both in Scotland, and WindFloat Atlantic in Portugal. In Asia, the first Chinese tri-floater based wind turbine has been deployed for demonstrative purposes off the coast of Yangjiang [6]. While these examples are tri-floater based, the spar based Hywind Tampen Wind Farm off the coast of Norway will be the biggest floating array with 88 MW in operation.

Development of floating wind farms presents unique and novel challenges to horizontal wind turbines (HAWTs). This is because reducing the levelised cost of energy (LCoE) and maintaining the structural integrity is increasingly difficult as the blades and the support structures increase in size. These issues become more relevant in modern HAWTs, as turbines can now be rated at 15 MW with blade lengths over 110 m [7]. In particular,

larger blades induce higher gravitational cyclic loading, putting at risk the reliability and structural integrity of the turbine. In addition to the structural complications, there are fluid dynamic considerations, such as, wind shear and turbulence, which play an important role and could alter the expected behaviour of a large-scale floating HAWT [8].

It has been hypothesised that an alternative to these challenges could be found in floating offshore vertical axis wind turbines (VAWTs) [9]. It is known that VAWTs have different characteristics from HAWTs [10–12]. For example, lower overturning moment and centre of gravity, and omnidirectional operation. However, to date, it remains unclear whether these characteristics could be beneficial in the context of large-scale floating VAWTs and whether it is worth diversifying turbine technology for floating arrays. To answer these questions, we compile and review a novel multi-criteria assessment from the offshore perspective. We address power capture, loading characteristics, floating support structures, reliability, environmental, manufacturing and decommissioning aspects of floating VAWTs. When relevant, we compare some of these aspects to those of floating HAWTs.

The structure of the paper is as follows. First, we provide a brief background on VAWT history and technology. Then, the multi-criteria assessment is presented. The analysis is finalised with a technology readiness level (TLR) assessment of floating VAWTs versus floating HAWTs. The way forward and conclusions are included at the end of the paper.

2. Novelty of the Review

The novelty of this review paper lies in the multi-criteria approach used to review VAWTs in the context of floating offshore technology. This contrasts with more conventional reviews that focus in one aspect only. An inclusive and multi-criteria approach is required in the literature to reach a broader range of stakeholders in industry, government and academia, that can influence decision making processes in the offshore energy mix. Then, we provide a range of solutions, together with research gap opportunities, to increase the TRL level of floating VAWTs. To do this we performed a TRL comparison between floating HAWTs and hypothetical floating VAWTs, where we identify specific areas of the latter that have a low TRL level. This allows us to focus the range of solutions in areas that will have an important impact on floating VAWT technology.

We intend that this review will raise awareness within the stakeholder and the research communities on which aspects could make floating VAWTs a complementary source of energy in the offshore energy mix. At the same time, we intend to highlight which areas need to be strengthened in order to make floating VAWTs a feasible alternative. As such, Figure 1 presents a flow chart that summarises the structure of this review.

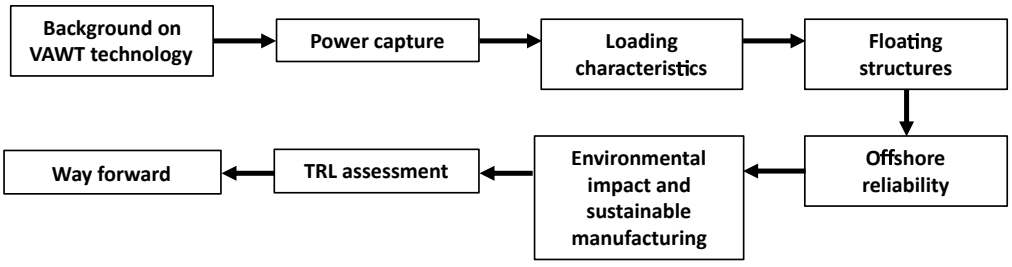

Figure 1. Flowchart of review showing the main blocks on: background on VAWT technology, power capture, loading characteristics, floating structures, offshore reliability, environmental impact and sustainable manufacturing, TRL assessment and way forward.

3. Background of VAWT Technology

VAWTs can be classified into four main types: Savonious, curved-bladed Darrieus, straight-bladed Darrieus and H-type turbines [13]. The former is drag-based, whilst the latter ones are lift-based turbines. Early developers in the 80s focused on the curved-bladed Darrieus turbine in North America and the H-rotor turbine in Europe and Asia [12,14]. Among the early developments, the largest VAWT was the Eole turbine in Canada. It

was a curved-bladed Darrieus turbine rated to 3.8 MW that operated for five years. The turbine worked with direct drive technology and had steel core blades, contrarily to most of its predecessors that operated with aluminium blades. High visibility failures of VAWTs due to fatigue issues in the main bearings and blades led to a loss in investment, which coincided with HAWT early success.

Trends have changed and recent years have shown a renewed interest in VAWT technology. VAWT small-scale developers (<0.1 MW), such as 4Navitas [15] and Swift TG Energy [16], have developed successful commercial onshore multi-bladed prototypes. Research and development of novel floating VAWT concepts have also been surging, for example, the cases of Nova [17,18], Deepwind [19], Skwid [20], Vertiwind [21] and SeaTwirl [22]. The latter is a Swedish company that aims to have an operational floating VAWT rated at 1 MW by 2023. Hence, efforts are under way towards larger-scale floating VAWT devices. We summarise some of these latest efforts in Table 1. As an illustrative example of a floating VAWT, Figure 2 shows the schematic of a floating straight-bladed Darrieus turbine supported by a tri-floater structure.

Table 1. Summary of floating VAWT research activity over recent years.

Name of Turbine	Type of Turbine	Country	Years Active	Reference
Nova	V-shape VAWT	UK	2009–2010	[17,18]
Deepwind	Curved-bladed Darrieus	Denmark	2010–2014	[19]
Floating axis	Straight/curved-bladed Darrieus	Japan	2011–ongoing	[23,24]
Skwid	Straight bladed Darrieus	Japan	2013–2015	[20]
Vertiwind	H-rotor	France	2011–2018	[21]
SeaTwirl	Straight-bladed Darrieus	Sweden	2012–ongoing	[22]

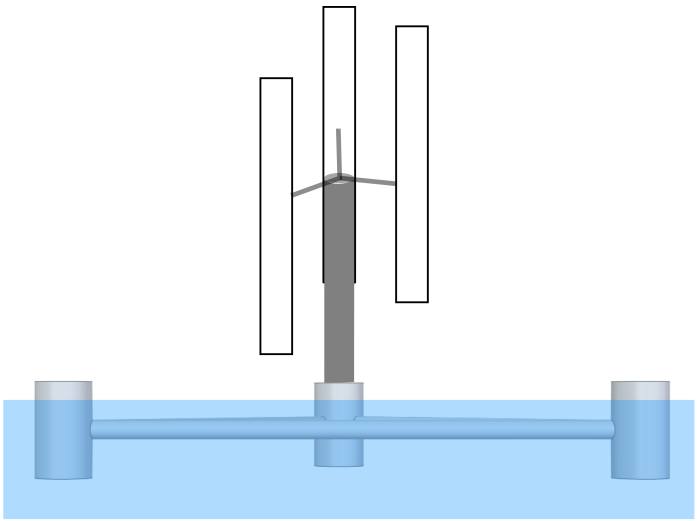

Figure 2. Schematic of a floating straight-bladed Darrieus turbine supported by a tri-floater structure.

4. Power Capture

In this section, we present an assessment of the power aspects of floating VAWTs and compare them to those of floating HAWTs from a single-machine and an array perspective. A priori, it is known that power capture capabilities from the individual machine perspective, differ significantly between VAWTs and HAWTs due to their principle of operation. For VAWTs, see for example, Hand et al. [25], and for HAWTs, see for example the Wind Energy Handbook from Burton et al. [26]. However, from the array perspective these differences might not be as relevant and we intend to explore this in this section. We start by describing the concept of power coefficient. Then, we discuss relevant parameters that can alter the performance of the turbines. Importantly, we discuss the swept area, the wind shear profile and the orientation of the turbine with respect to the wind. Subsequently, we

discuss an example of array performance by quantifying the power density of two wind farms, one with floating HAWTs and one with floating VAWTs.

4.1. Power Coefficient

One of the factors that determined the early success of HAWTs over VAWTs was the power coefficient (C_P). The C_P is the percentage of wind energy that a turbine can convert into electrical energy [26]. It is defined as

$$C_P = \frac{P}{0.5\rho A U^3}, \quad (1)$$

where P is the extracted electrical power, ρ is the fluid density, U is the freestream velocity and A is the swept area of the turbine. The denominator in Equation (1) is the available power through the swept area of the turbine. A typical value for the maximum power coefficient ($C_{P,max}$) of a HAWT is around 0.5, with the Betz limit ($C_P = 16/27$), as the theoretical upper limit. For a lift-based VAWT, a typical value of $C_{P,max}$ is around 0.4. These values are only valid for isolated machines, and in the case of HAWTs, only valid in uniform unidirectional flow. Orientation of the turbines with respect to the flow is discussed further in Section 4.4.

Table 2 shows examples of a HAWT, a Darrieus and an H-rotor. The table shows the $C_{P,max}$ and the corresponding tip speed ratio λ for each turbine. Here, λ is defined as $\lambda = \omega r/U$, where ω is the angular velocity of the turbine and r is the radius, i.e., λ is the ratio between the tip speed of the blade and the free-stream velocity. In the table, the HAWT case corresponds to the NREL 5 MW turbine [27]. The $C_{P,max}$ was computed with the open source software Q-blade [28] and is confirmed against literature data [29]. The Darrieus $C_{P,max}$ is that published by Sandia laboratories for the 34 m diameter turbine tested in the late 80's [30,31]. Whilst, the $C_{P,max}$ from the H-rotor is obtained from Eriksson et al. [11] and corresponds to the two-bladed British VAWT 260, rated at 100 kW [32]. The table shows the superior performance of the HAWT turbine. The $C_{P,max}$ of the VAWT turbines is similar, except that $C_{P,max}$ of the H-rotor occurs at a lower λ.

Table 2. HAWT and VAWT turbines with characteristic $C_{P,max}$ and corresponding λ. The source of the data is specified in the last column.

Turbine	Power Rating	Type of Turbine	$C_{P,max}$	λ	Data from
NREL	5 MW	HAWT	0.49	8.0	Qblade simulation
NREL	5 MW	HAWT	0.48	7.9	Zanon et al. [29]
Sandia 34 m	500 KW	VAWT-Darrieus	0.40	6.1	Sandia report [30,31]
Musgrove	100 KW	VAWT-H-rotor	0.40	3.8	Eriksson et al. [11]

We note that the value of $C_{P,max}$ for VAWTs depends also on the solidity of the turbine (σ) [33] and on the Reynolds number (Re) [34]. Typically, σ is defined as $\sigma = Nc/r$, where N is the number of blades and c is the mean chord of the blade. Low σ ($\sigma \leq 0.1$), decreases $C_{P,max}$ and increases its corresponding λ. In contrast, high σ ($\sigma \geq 0.4$), increases $C_{P,max}$ and decreases its corresponding λ [33]. In terms of Re, low Re decreases $C_{P,max}$ [34]. However, for large-scale floating offshore VAWTs, we expect high Re ($Re > 1 \times 10^5$) and therefore, a consistent $C_{P,max}$ over the range of 0.4 to 0.45 [34].

4.2. Swept Area

The swept area of the turbine A can be modified to alter P, as shown by Equation (1). Different design strategies can be utilised to set A, and hence P of a turbine. As an example, here, we show A of turbines of similar height in Figure 3. We delimit the A of a HAWT, a Darrieus and a H-rotor turbine with a dotted blue, black and red line, respectively. The HAWT A has the dimensions of the 5 MW NREL rotor [35], whilst A of each turbine is overlapped with the zero defined at mid-height of the turbines. For HAWTs and Darrieus turbines, the height to diameter ratio (h/d) is fixed to $h/d = 1$ and $h/d = 1.5$, respectively.

In contrast, h/d for an H-rotor can vary over a wide range. In fact, it is theoretically possible to size an H-rotor to match the P of a similar height HAWT, by adjusting its diameter only.

From Table 2, we consider a $C_{P,max}$ = 0.4 for the Darrieus and the H-rotor turbine, and $C_{P,max}$ = 0.48 for a HAWT. We compute P for each turbine by utilising Equation (1). A reference offshore height and reference offshore wind velocity is defined for each turbine. For the HAWT, the reference height is the hub height at 90 m, whilst the wind rated velocity (U_r) is 11.4 m/s [35]. For the VAWTs, we consider a reference height equal to half of the height of the turbine plus a 10 m distance to the sea level. By assuming a power law and a power law coefficient $\alpha_l = 0.11$ [36], we can compute U_r for the VAWTs. This yields $U_r = 11.3$ m/s and $U_r = 11.2$ m/s for the Darrieus and the H-rotor, respectively. Under these assumptions, the turbines are rated to 5 MW, 4 MW and 5 MW for the HAWT, Darrieus and H-rotor, respectively.

Hence, in this example, it is shown that an H-rotor of equal or similar height to a HAWT can match the P of a HAWT, even with a lower $C_{P,max}$.

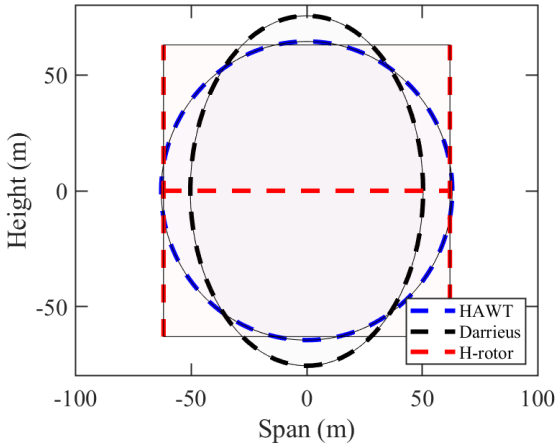

Figure 3. Swept areas (A) of HAWT (blue dotted line), Darrieus (black dotted line) and H−rotor (red dotted line). The rated velocities (U_r) are 11.4, 11.3 and 11.2 m/s, whilst P is 5, 4 and 5 MW, respectively. For these computations, we utilised $C_{P,max} = 0.48$ for the HAWT, and $C_{P,max} = 0.40$ for the VAWTs.

4.3. Wind Shear Profile

Although in the previous subsection, we utilised a power law, wind shear profiles can also be modelled with a log law [37] or with a simplified log law [38]. The characteristic equations of the power law, power log and simplified power log, can be found, for example in Sathe and Bierbooms [39] or in Golbazi and Archer [38]. For the log law, the offshore surface roughness is typically $z_0 = 0.001$, whilst onshore, surface roughness can range between $0.03 \leq z_0 \leq 0.7$ [26]. For the power law, the offshore power law exponent is typically $\alpha_l = 0.11$, whilst onshore, the power law exponents can range between $0.14 \leq \alpha_l \leq 0.25$ [40].

By utilising a reference height of 90 m and a reference velocity of 11.4 m/s, it can be shown with the power law and the simplified log law, that offshore, around 80% of the rated wind speed can be reached at 10% of the reference height. In contrast, between 50% to 70% of the rated wind speed (depending on the flatness of the terrain) is achieved at the same height in onshore conditions. This means that, in theory, the power extracted offshore by a floating VAWT can be higher than the power extracted by the same VAWT onshore. Hence, the shape of the offshore wind profile becomes a significant advantage for floating VAWT deployments.

4.4. Orientation of Turbine towards Wind

Orientation of the turbine towards the wind direction is important for HAWT performance. Yaw misalignment (γ) occurs when the rotor plane of the turbine is not perpen-

dicular to the wind direction. In fact, γ reduces the power of a turbine proportionally to $\cos^k\gamma$, where $k = 3$ assuming uniform flow and thrust. In reality, $k \neq 3$, because it is site and turbine model specific [41]. A common metric to quantify the effects of γ in HAWTs is the power ratio P_r, which is the ratio between the yaw misaligned P and the yaw aligned P [41].

Table 3 shows the effect of γ in P_r of a HAWT and a VAWT. For a HAWT, P_r is computed with $\cos^3\gamma$ and $\cos^2\gamma$, where the former is assuming uniform loading and thrust and the latter is the correction suggested by Howland et al. [41]. For a VAWT, P_r = 1.00 because of its γ independence. The table shows that γ is detrimental for the performance of HAWTs. In fact, when $\gamma = \pm 30°$, P_r can drop to about 65% to 75%.

Table 3. Effect of γ in P_r for a HAWT and VAWT. For a HAWT, P_r is computed with $\cos^3\gamma$ and with $\cos^2\gamma$. The latter is a correction suggested by Howland et al. [41].

γ [°]	**HAWT Uniform Thrust** $P_r = \cos^3\gamma$	**Suggested by Howland et al. [41]** $P_r = \cos^2\gamma$	**VAWT Theoretical** $P_r = 1$
±5	0.99	0.99	1.00
±10	0.96	0.97	1.00
±15	0.90	0.93	1.00
±20	0.83	0.88	1.00
±25	0.74	0.82	1.00
±30	0.65	0.75	1.00

To mitigate the drop in P_r, HAWTs can yaw into the wind direction. There is, however, a mechanical limit on how much a HAWT can yaw. Typical values range over ±30° [42]. Assuming $\cos^2\gamma$ and a maximum yaw correction of 30°, wind changes higher than 45° can reflect in a drop in P_r of about 10%. In the North Sea, wind changes of 90°, away from the average wind direction, are to be expected [43]. These events can yield a HAWT wind farm inoperative [44] and can extend to half of the total yearly hours [43]. In contrast, because VAWTs are omnidirectional, they can capture the wind from any direction. This increases reliability, because no yaw system is required, and eliminates losses in P_r due to γ. Reliability and simplicity are preferred for floating offshore deployments, where complex systems, such as yaw systems, might incur higher failure rates and downtimes [45]. Reliability is discussed further in Section 7.

4.5. Wind Farm Power Density

Wind farm power density (ρ_{WF}) is a metric that quantifies how much power per square metre a wind farm produces. VAWTs can be placed next to each other in counter-rotation in the crosswind direction [46], whilst in the downwind direction a spacing between 4 to 8 diameters could be enough for the wake to recover above 80% [47–49]. In contrast HAWTs require a distance of 8 and 10 diameters in the cross-wind and in the downwind directions [50], respectively, to achieve $C_{P,max}$. Hence, for turbines with similar height, as with those shown in Figure 3, ρ_{WF} of a floating VAWT wind farm can be superior to that of a HAWT wind farm. Neglecting losses and assuming a wind farm capacity factor $CF_{WF} = 1$, ρ_{WF} can be defined as

$$\rho_{WF} = \frac{\text{power per wind turbine}}{\text{offshore area per turbine}}. \quad (2)$$

The power per wind turbine is the electrical power of the turbine P, which is given by Equation (1). The offshore area per turbine is computed assuming a circular footprint of radius equal to the spacing of the turbines [51] or a radius equal to half the spacing of the turbines [47]. Because the footprints should not overlap, here we use the latter definition to estimate the power density of the wind farms of Figure 4. The figure shows a HAWT wind farm with 10D downwind spacing and 8D crosswind spacing, as specified by Musial [50], and a VAWT wind farm of H-rotors, where we take a conservative approach in the cross-wind direction and space the turbines 6D apart. Whilst in the downwind direction, we

consider 6D, as the average recovery value that we found in the literature [47–49]. For the HAWT wind farm, we take an average spacing of $9D$, in both directions, to estimate ρ_{WF}.

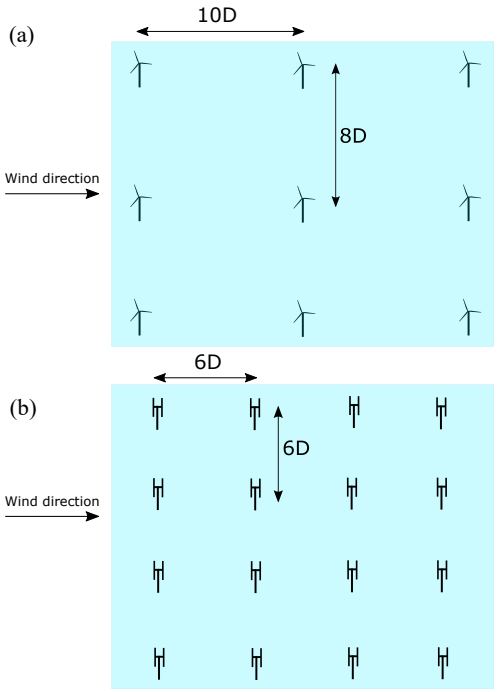

Figure 4. Wind farm spacing layout of (**a**) HAWTs and (**b**) VAWTs, considering wake recovery requirements and assuming uniform wind direction.

Utilising D of the HAWT and H-rotor turbines plotted in Figure 3, the computed ρ_{WF} for the HAWT wind farm is 5 W/m^2, whilst for the VAWT wind farm is 12 W/m^2. Hence, these two layouts show that 16 floating VAWTs placed closer to each other can outperform 9 floating HAWTs placed further apart. We note that the VAWT wind farm would still outperform the HAWT wind farm by 30% if the downwind direction was increased to 8D [49]. Furthermore, downwind spacing could be decreased to 5D if counter-rotation was to be employed [46]. This would automatically double ρ_{WF} due to the pairs of turbines working at every node of the wind farm.

Naturally, more populated wind farms are not desirable due to more installation trips. Indeed, reducing the number of installations reduces the CAPEX cost of the wind farm. However, because the power density of a VAWT wind farm would increase the annual energy output (AEP), the wind farm would also decrease its levelised cost of energy (LCoE). Furthermore, because of the lower centre of gravity of VAWTs (see Section 6.2), towing speeds could be increased, and possibly, a reduced number of towing vessels could be used per floating VAWT. Therefore, it could be possible to minimise the impact of more installations per wind farm, by an increase in AEP due to higher ρ_{WF} and omnidirectional operation of VAWT wind farms.

5. Loading Characteristics

This section presents a summary of the loading characteristics that a VAWT turbine encounters during a cycle of rotation. We highlight the aspects that become relevant for floating VAWTs.

Figure 5 shows a mid-height cross section of a two-bladed VAWT and the velocity triangle of each blade. The direction of the wind is from left to right and the upstream and downstream half cycles are highlighted with blue and red shaded areas, respectively. The x-axis points in the wind direction, whilst the y-axis points downwards. The rotation of the turbine is in the clockwise direction.

In the figure, V_{tan} is the tangential velocity, V_{in} is the induced velocity, V_{rel} is the relative velocity on each blade, r is the radius of the cross-section and θ is the azimuthal angle with respect to the y-axis. Hence, blade 1 is at $\theta = 90°$ and blade 2 is at $\theta = 270°$. The force components on each blade are lift and drag (F_L, F_D), and the tangential and radial force components (F_T, F_R).

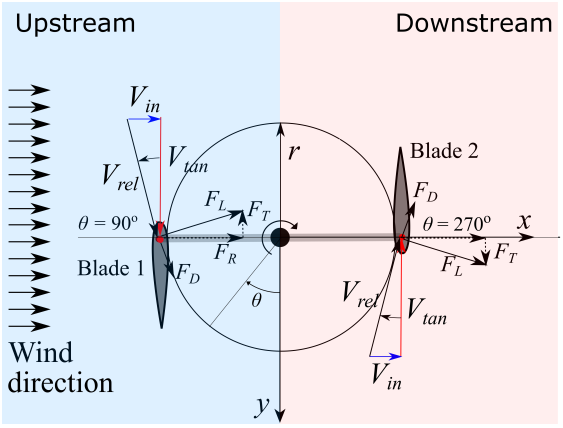

Figure 5. Schematic diagram of a cross-section of a two-bladed VAWT.

The flow slows down as it approaches the turbine in the upstream half-cycle and also due to blade-wake interactions in the downstream half-cycle. This causes an asymmetric oscillation on the angle of attack of the blade α between the upstream and the downstream half-cycle. Hence, due to the complex blade-flow interactions, different analytical models have been developed to estimate the loads of VAWTs. For example, single stream tube actuator disc models [52], multiple stream tube double disc theories [53,54], actuator cylinder models [55,56], potential flow vortex models [57,58], cascade models [59] and recent adaptations of helicopter unsteady models [60]. Most of the models include corrections for dynamic stall, wind shear, strut drag and tower shadow. A summary of some of the models can be found, for example, in Islam et al. [13]. Recent years, have also seen computational fluid dynamics (CFD) expanding the understanding of the unsteady loading of VAWTs [34,61,62], albeit at the cost of an increased computational cost.

For floating offshore VAWTs, hydro-aerodynamic coupled models have been successfully implemented [63–65], but presently they are scarce in the literature. However, validation data for coupled systems is not available, hence the models are typically validated modularly, and against each other.

In this paper in order to gain an insight on the loading characteristics of VAWTs and assess the potential impact of relevant design parameters in floating VAWTs, we study the geometric angle of attack α_g. We note that α_g neglects variations of V_{in}, however, basic aerodynamic characteristics, as well as the cyclic nature of the loads can be analysed to understand potential implications for floating VAWTs. For details on how to calculate α_g the reader is referred, for example, to [13,34]. We note that in the computations of α_g, V_{in} is assumed to be equal to the freestream velocity.

The first important design parameter that influences α_g is λ. Low λ decreases the magnitude of V_{tan} and increases α_g, while it also makes the α_g oscillations asymmetric. In contrast, high λ, decreases the amplitude of α_g and makes the oscillations more symmetric. These effects are illustrated in Figure 6a which shows α_g of one VAWT blade during a full azimuthal rotation, plotted at $\lambda = 2.5, 3.5$ and 4.5. We utilise the dimensions of the VAWT turbine tested by LeBlanc and Simao Ferreira [66] and provide a Matlab script as supplementary material to produce Figure 6a. The optimal λ is one that prevents dynamic stall and that is not detrimental to the fatigue life of the blades (high α oscillations), but also, one that prevents low power output (low α oscillations).

The oscillations in α_g result in torque (Q) and thrust (T) oscillations in a two-bladed VAWT. Specifically, the Q and T oscillations are due to the oscillations in F_T and F_R of the

blades, respectively. The Q oscillations are typically referred to as the torque ripple [31,67], whilst examples of T oscillations can be found in [66,68]. Both T and Q oscillations need to be minimised in floating offshore VAWTs. This is because oscillations in T can amplify pitching motions, whilst oscillations in Q can induce torsional moments and affect the fatigue life of the mooring lines.

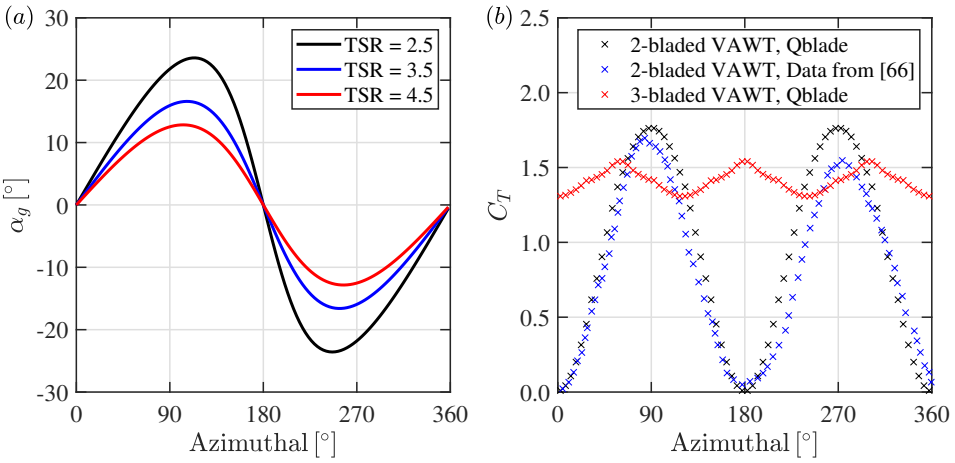

Figure 6. (**a**) Oscillations of α_g at $\lambda = 2.5, 3.5$ and 4.5 during one rotation cycle for one VAWT blade. Turbine dimensions are those used in [66]. (**b**) C_T versus rotor azimuthal angle at $\lambda = 3.5$ for a two-bladed VAWT, simulated with Qblade and experimental data from [66] in black and blue markers, respectively. The red markers show the simulated C_T, with Qblade, for a three-bladed VAWT.

We illustrate the oscillating nature of the loads in a two-bladed VAWT by plotting the thrust coefficient (C_T) versus the azimuthal angle of the rotor in Figure 6b. We utilise the open-source software Q-blade to compute C_T of a two-bladed turbine with the same dimensions as the one tested experimentally by LeBlanc and Simao Ferreira [66] for λ = 3.5. Results of the simulation are plotted with black markers. For reference, we include the experimental results with blue markers. Two peaks in C_T are noted at 90° and 270°.

In contrast to two-bladed VAWTs, multi-bladed VAWTs smooth out the two peak loading oscillations [67]. In fact, modern onshore small-scale VAWT manufacturers utilise multiple blades in their designs. Multi-bladed VAWTs are also applicable for floating offshore VAWTs, where cost increments due to a third blade could be compensated by an increase in AEP (see Section 4) and also, by a reduced complexity in the manufacturing of the blades (see Section 8.2). In Figure 6b, we show with red markers the C_T of a three-bladed VAWT computed with Qblade. As shown in the figure, the oscillating peaks are smoothed out compared to the peaks of the two-bladed case. Reduced oscillations are a more desirable scenario for floating arrays to minimise load induced motions and extend the fatigue life of the turbine.

6. Floating Structures

In this section, we identify the existing types of support structure in the offshore market. As well as the current trends in floating turbine deployment. Subsequently, we present a free floating body diagram to highlight the importance of a low centre of gravity (CoG) and a low overturning moment (OTM), and put this into the context of floating turbines. Finally, we quantify the potential reduction in OTM with a practical example.

6.1. Types of Floating Structures

Floating offshore structures should provide enough buoyancy to support the turbine and restrain pitching, rolling and heaving motions [69]. Several floating technologies exist and have been successfully used in the offshore oil and gas sector. Hence, the technology

readiness level (TLR) of floating structures is high. The challenge lies in designing a floating structure that operates in conjunction with the VAWT turbine.

Examples of floating structures are: barges, semi-submersibles, spar buoys and tension mooring legs (TLPs). Barges are flat floating platforms typically used to transport cargo offshore. Semi-submersibles are platforms supported by floats. They are typically used for deep water offshore drilling. The floats are airtight hollow structures designed to provide buoyancy. They provide an improved stability compared to barges, due to their reduced water plane. Spar buoys are elongated bodies that are ballasted at the bottom to lower the CoG and improve stability. Whilst, TLPs are floating structures moored to the seabed by high axial stiffness tethers. The tethers minimise vertical motions of the platform and are attached to the seabed through specialised anchors. A technical assessment of some of these floating structures can be found, for example, in [27].

The stability triangle, shown in Figure 7, is generally used to classify floating structures according to their stability mechanism [68,69]. The vertices of the triangle are: buoyancy, ballast and mooring supported structures. Locations between vertices are used to classify hybrid types of support structures. We utilise the triangle to highlight some floating VAWT concepts that have been developed recently by both academia and industry. Representative symbols are used to identify the type of floating VAWT system (semi-sub, spar buoys and TLPs). The figure shows that most of the identified floating VAWTs are buoyancy and ballast supported. Hybrid mechanisms, that combine buoyancy and ballast supported turbines, are the cases, for example, of Deepwind [19] and the floating axis wind turbine (FAWT) [23,24]. For comparison, some of the already deployed floating HAWT wind farms are plotted in the figure. We note that most of these large-scale developments have also leaned towards buoyancy and ballast supported mechanisms. Mooring supported systems, such as TLPs, remain vastly unexplored for both HAWTs and VAWTs. One exception to this is Seawind [70], which is a two-bladed HAWT supported by a TLP.

Most of the identified cases in Figure 7 are on the leftward side of the triangle. We consider that the two main drivers behind this trend are: the installation costs and the geographic location of the port where the turbine is assembled.

The first driver is evidenced in a recent life-cost analysis for semi-subs, buoy spars and TLPs [71]. In summary, the main costs related to a floating structure are: manufacturing, operation and maintenance, and installation. Among these aspects, the greatest differentiator between platforms is the installation cost. For TLPs, the cost is higher because they typically require suction or driven piles to keep the mooring lines in tension and provide the required vertical load. Furthermore, they require cargo barges and offshore lift cranes for installation [71].

The second driver is of a geographical nature, since floating structures of large draft, such as spar buoys, can only be assembled near shore in certain locations. This is because offshore assembly increases costs significantly. In the UK, for example, deep water quays in the range of 20 to 25 m are non-existent [72]. Hence, assembly of semi-subs and spar buoys is not feasible. Contrarily, quaysides in Norway allow for assembly of semi-subs and spar buoys with drafts longer than 50 m. Such is the case of the deep water site of Dommersnes, where Hywind Tampen is being assembled [73]. In addition to water depth restrictions, the location of the port needs to be in the vicinity of the wind farm. Proximity to offshore site reduces the duration and cost of the trips to the site. Hence, location and proximity of the assembly port to the wind farm are major drivers behind the chosen type of floating platform.

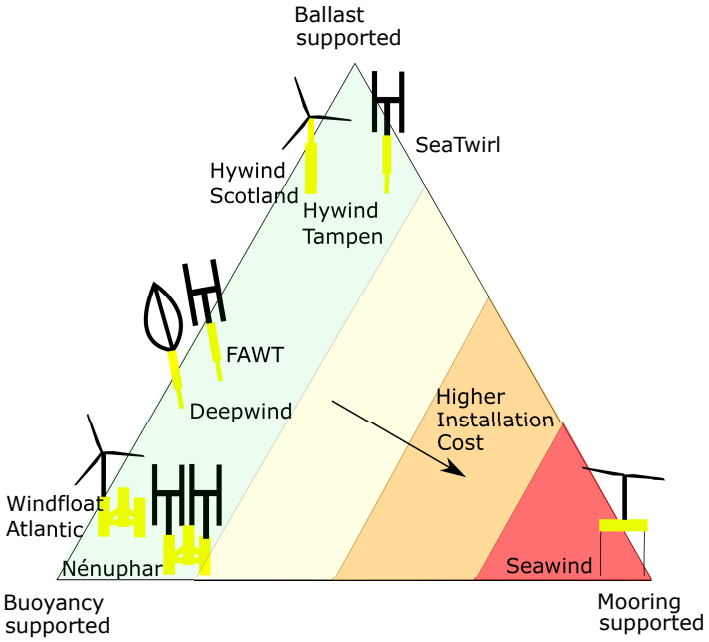

Figure 7. Stability triangle with buoyancy, mooring and ballast supported structures at the vertices of the triangle. Examples of floating VAWTs and HAWTs are identified in the figure. The colour bar in the triangle indicates installation costs, with costs increasing from light green to red.

6.2. Stability

VAWTs have two significant advantages for floating offshore deployments. Firstly, a lower line of action of the average thrust force ($\overline{T}$) and secondly, a lower centre of gravity (CoG).

We illustrate both points in Figure 8. The figure shows a free floating structure whose symmetry lines are initially aligned with the vertical y-axis and the horizontal x-axis. The contour of the structure is highlighted with a black dotted line in this reference frame. The structure is then tilted around the pitching axis O and the symmetry lines are now aligned with the x' and the y'-axis. In the figure, the tilted structure is shaded in pink. The figure shows the weight of the structure (W), the centre of gravity (CoG), the buoyancy force (B), the centre of buoyancy (CoB), the overturning moment (OTM), the restoring moment (RM) and the pitching axis O. We note that W acts on CoG, B on CoB and that RM is the moment due to B and W around O. Similarly, OTM is the moment due to $\overline{T}$ around O.

We specify, the average thrust force of a HAWT and of a VAWT as $\overline{T}_{\mathrm{HAWT}}$, and $\overline{T}_{\mathrm{VAWT}}$, respectively. These forces are applied at different points along the y'-axis, which represent the height where the thrust force acts. Specifically, the line of action of $\overline{T}_{\mathrm{HAWT}}$ is hub-height, whilst the line of action of $\overline{T}_{\mathrm{VAWT}}$ is approximately mid-height of the turbine. Assuming similar height turbines, such as those depicted in Figure 3, the OTM due to $\overline{T}$ around O is lower in a VAWT than in a HAWT. This reduces the restoring moment (RM) and structural requirements needed to balance OTM, and sustain the stability of the structure.

Secondly, a lower CoG increases the restoring moment (RM) experienced by the floating structure. This is because the position of the CoG remains fixed at the symmetry line of the structure, assuming there are no free weights that can move [74]. Therefore, the distance between the CoG and the untilted vertical axis (y-axis) increases with a lower CoG. This distance is the lever arm of the moment due to W around O. We refer to the moment and the lever arm distance as M_{W} and l_{CoG}, respectively. Hence, $M_{\mathrm{W}} = \mathrm{W} \times l_{\mathrm{CoG}}$.

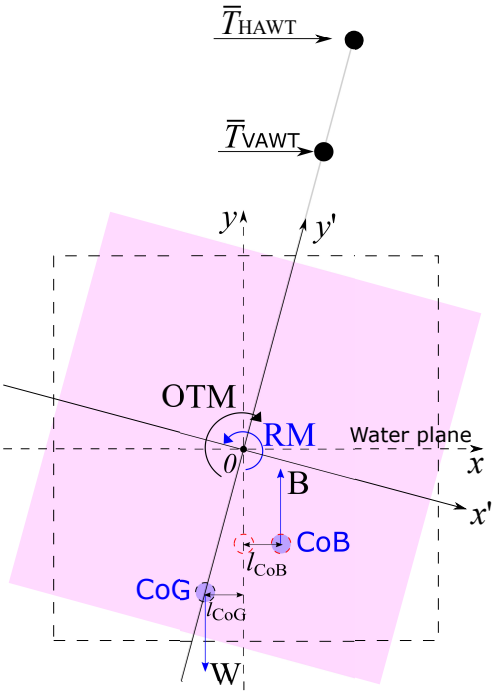

Figure 8. Schematic of a free floating wind platform, with the overturning moment (OTM), due to average thrust force ($\hat{T}$), and the restoring moment (RM), due to buoyancy and gravity forces acting at the centre of buoyancy (CoB) and gravity (CoG), respectively.

The moment due to the buoyancy force is $M_{\mathrm{B}} = \mathrm{B} \times l_{\mathrm{CoB}}$, where l_{CoB} is the distance from the CoB to the y-axis. We note, that the position of the CoB changes after tilting due to a change in the underwater shape of the structure. The change in the position of the CoB is illustrated in the figure, where the CoB moves from the untilted symmetry line (red dotted circle) to the right hand side of the y-axis. Finally, RM around O is RM $= M_{\mathrm{W}} + M_{\mathrm{B}}$. VAWTs can have heavy equipment, such as the generator and the gearbox positioned closer to sea level and therefore a lower CoG. The ability to have a lower CoG decreases the amount of ballast material that a floating structure requires to lower the CoG. This reduction in material can translate into a reduction in the cost of the floating structure.

We quantify the potential reduction in OTM of VAWTs rated at different P. To this aim, we compare the OTM of three different large-scale turbines. We consider the HAWT, Darrieus and H-rotor turbines. The scaling of the HAWT turbines is performed taking as reference the A of the 5 MW NREL turbine depicted in Figure 3, and scaling A to match the desired P. We consider $C_{P,\mathrm{max}} = 0.48$ and $C_{P,\mathrm{max}} = 0.40$ for HAWTs and VAWTs, respectively. The scaling for the VAWTs is performed by considering the scaled-up HAWTs and keeping the same height and h/d ratio relationships between the HAWT and VAWT turbines that are utilised in Figure 3.

The dimensions of the turbines are provided in Appendix A and they are grouped in three clusters: A, B and C, which refer to medium ($\leq$5 MW), large ($\leq$10 MW) and very large-scale (>10 MW), respectively. The rated velocities (U_r) for each turbine is provided in Appendix A. The velocities are computed with a power law and a reference wind velocity of 11.4 m/s at 90 m above sea level [35]. The reference heights for U_r are hub-height for the HAWTs, and mid-height plus a distance of 10 m above sea level for the VAWTs. The power law coefficient is $\alpha_l = 0.11$, as previously specified for offshore sites [36].

Results are shown in Figure 9. The figure shows the estimated OTM versus P of the turbines of cluster A, B and C. Circular, diamond and rectangular markers are used to represent the HAWTs, Darrieus and H-rotor turbines. Despite the apparent disadvantages of VAWTs (lower U_r and lower C_{P}, we note that the H-rotor matches the P of the HAWTs in clusters A and B, and is only slightly under rated in cluster C. In contrast, the Darrieus turbines do not match the P of the HAWTs in any of the clusters.

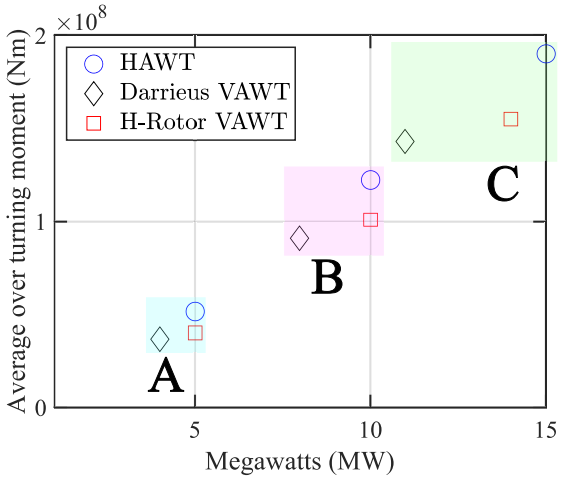

Figure 9. Average overturning moments (OTMs) for clusters A, B, C corresponding to medium, large and very large-scale turbines, respectively. Each cluster considers a HAWT, a Darrieus and a H-rotor turbines, whose dimensions are provided in Appendix A.

A reduction in OTM is observed for VAWTs in all of the clusters. The reduction in OTM between HAWTs and the H-rotor increases from cluster A to cluster C, from 5% to about 20%. Hence, the OTM decreases with increasing H-rotor power. For the Darrieus rotor, a reduction in OTM is observed in every cluster, ranging over 25% to 30%, although this comes at the penalty of turbines with a lower rated P. We recall however that due to omni-directionality and tighter arrays capability, any P deficit in the clusters could be overcome. Furthermore, HAWTs cannot produce power all the time, as pointed out in Section 4.4. Hence, the annual average power output of a HAWT is much less than the rated power [44].

Lastly, it is worth noting that the reduction in OTM of the H-rotor is more significant if $h/d < 1$, provided that A is sized according to the required P. We note that in the examples of Figure 9, $h/d = 1$ for the H-rotor.

7. Offshore Reliability

Up to this point, we have reviewed power capture capabilities of floating VAWTs from an individual and array perspective. We subsequently studied some of their loading characteristics. Then, we reviewed the available floating platforms and highlighted that floating VAWTs have an improved stability due to a lower CoG, and a lower OTM. In this section, we focus on the reliability of aspect in the context of a floating platform.

Reliability of wind turbines is crucial to reduce operation and maintenance (O&M) costs associated to failure rates and downtimes [75]. This has led to several studies to investigate the failure rates and downtimes of onshore and offshore wind turbines [45,76–78]. However, to date, offshore reliability databases are scarce, due to the competitive nature of the business. In addition to scarce data, the available information has high variability. This is because of the different sample sizes and locations [45].

Despite these shortcomings, some insight can be gained from offshore reliability databases and relevant conclusions applicable to floating VAWTs can be obtained. Here, we review three offshore databases reported by Dinwoodie and McMillan, Carroll et al. and Dao et al. [45,76,77]. These studies show that the highest offshore failure rates typically occur in pitching systems, generators, gearboxes, yaw systems and blade-hub assemblies. Figure 10 shows the box and whisker plot of the yearly percentage failure rate of these subcomponents, as reported in the aforementioned databases. The minimum and maximum points of each box correspond to the Dinwwoodie and McMillan, and the Dao et al. databases, respectively, with the exception of the yaw category, where this pattern is inverted. Figure 10 shows that the failure rate of these components account for about 50% of the total failure rate of an offshore HAWT wind farm.

Figure 11 shows the associated downtime hours related to the same subcomponents presented in Figure 10. The longest downtimes are due to the generator, the gearbox, and the blades-hub categories. It is noted that the variability is high in these three categories.

In contrast, pitch and yaw systems show lower downtimes and less variability. By multiplying the mean failure rates and the mean downtimes of Figures 10 and 11, and by normalising the results, we produce the severity matrix shown in Figure 12. The matrix highlights the impact of a failure in a floating HAWT. In the matrix, the severity of the failure is ranked as low ($0 < \text{low} < 0.2$), medium ($0.2 < \text{medium} < 0.5$) and high ($\text{high} \geq 0.5$). The matrix shows that failures in the generator and gearboxes have a high severity, whilst failures in the pitch, yaw and blade/hub systems are less severe.

We use the outputs of the severity matrix to derive some conclusions for floating VAWTs. We observe that VAWTs can minimise or eliminate the medium to low risk associated to yaw and pitch systems. Furthermore, the ease of accessibility to the generator, together with novel direct drive technology [79] could result in mitigation of the severity of the failures associated with generator and gearbox. Lastly, we note that although mechanical breaks are not identified as a primary source of failure and downtime rate, the lower λ of VAWTs can reduce the wear of the breaks and therefore mitigate any break-related fatigue issues.

The potential reduction in downtimes and failure rates of floating VAWTs, in combination with a higher ρ_{WF}, could help to decrease the levelised cost of energy (LCoE) of a wind farm, by lowering operational expenditures and increasing the annual energy production (AEP).

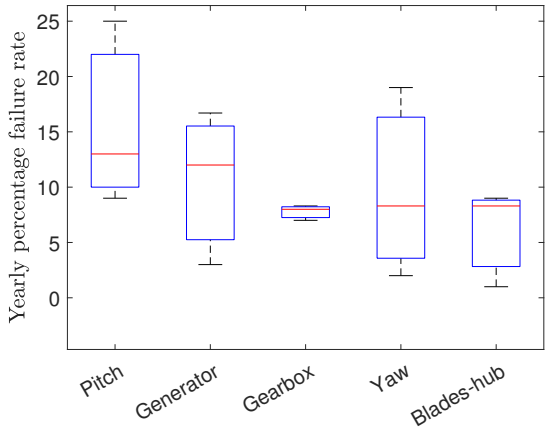

Figure 10. Box plot of components with higher failure rates for HAWT offshore wind farms. Data from Dinwoodie and McMillan, Carroll et al. and Dao et al. [45,76,77].

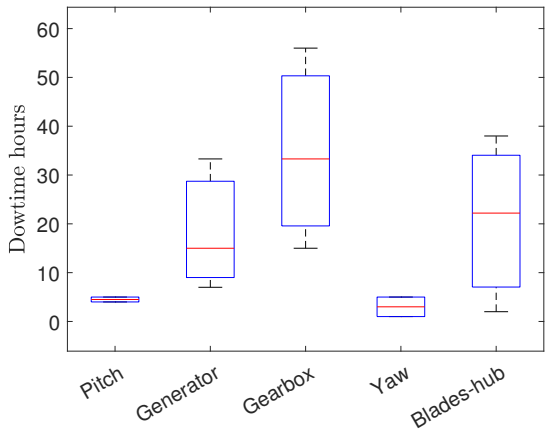

Figure 11. Box plot of downtime of components with higher failure rates for HAWT offshore wind farms. Data from Dinwoodie and McMillan, Carroll et al. and Dao et al. [45,76,77].

	High	Medium	Low
Pitch		0.26	
Generator	0.72		
Gearbox	1.00		
Yaw			0.11
Blades/hub		0.47	

Figure 12. Severity risk matrix of normalised failure rates times downtime rates for pitch, generator, gearbox, yaw and blade/hub in an offshore HAWT wind farm, as computed from box plots of Figures 10 and 11.

8. Environmental Impact and Sustainable Manufacturing

This section wraps up the reviewed features of floatings VAWTs, by analysing some of their environmental, manufacturing and decommissioning aspects. Subsequently, we carry out the TRL assessment to identify areas of opportunity and research gaps in the field of floating VAWTs.

8.1. Environment

Wind farms can influence their surrounding environment through electromagnetic interference, visual acceptability, bird collisions, noise, microclimates, etc. [80]. Offshore, some of these aspects become less critical, such as visual acceptability or noise. However, other aspects, such as bird collisions, remain a concern due to the growing size of HAWT turbines. Marine bird species such as seagulls, grebes, seaducks, migrating waterfowls and passerines [81] are at higher risk of collisions during migration or foraging activities.

Although it has been stipulated that VAWTs may have a lower impact on bird collision [82,83], further research on this area is still needed [84]. There are, however, some mitigation strategies that have been proposed to reduce bird collisions in wind farms [81,85–87]. Among the proposed strategies, reduction of wind farm footprint and parallel alignment to flight paths are possibilities for offshore VAWTs. As mentioned in Section 4.5, offshore VAWTs have the ability to be placed closer to each other in both cross-wind and downwind directions. This ability would allow a reduced wind farm footprint and potential alignment of the turbines parallel to the flying paths of birds.

In addition to physical collisions, wake interference is also an issue for birds and light aircraft [88]. The wake of HAWTs can cause undesired rolling moments and therefore bird and light aircraft collisions. As HAWTs grow in size, the dimensions of the wake and the likelihood of wake interference grow as well. It is possible to mitigate wake interference effects by having more compact arrays in counter-rotation and by reducing the height of VAWT turbines. The loss of power due to lower turbine heights, could be compensated by a higher ρ_{WF} and in the case of H-rotors, also by an increase in their diameter.

8.2. Sustainable Manufacturing

VAWT blades have uniform spanwise cross-sections, in contrast to non-uniform spanwise cross-sections of HAWT blades. As an example we illustrate in Figure 13a the side-view of the NREL 5 MW HAWT blade with 4 cross-sections highlighted throughout the span from root to tip. Whilst, Figure 13b shows the cross-section of an H-rotor with a symmetric NACA profile. The figure highlights the simplicity of VAWT blades compared to that of HAWT blades.

Although blade segmentation has been proposed for large HAWT blades, the non-uniform cross sections and high cyclic loading due to gravity pose significant structural challenges to the blade manufacturing process. Hence, HAWT blades are typically manufactured in a mould and in one single piece. In comparison, segmentation and modular assembly of VAWT blades is simpler because of the uniform cross-section and because of

the reduced gravity cyclic loading on the blade. Modularity in manufacturing can translate into significant cost reductions [10,89].

Modular assembly opens up the possibility for new materials for blades in VAWTs. For example, lighter materials based on sailing textiles, such as those proposed by company Actblade [90]. Lighter materials can reduce the weight of the blade and any gravity-induced pitching motion on the floating structure. They can also reduce the loading on the supporting struts of the blades. Simultaneously, novel materials can provide a sustainable recycling framework.

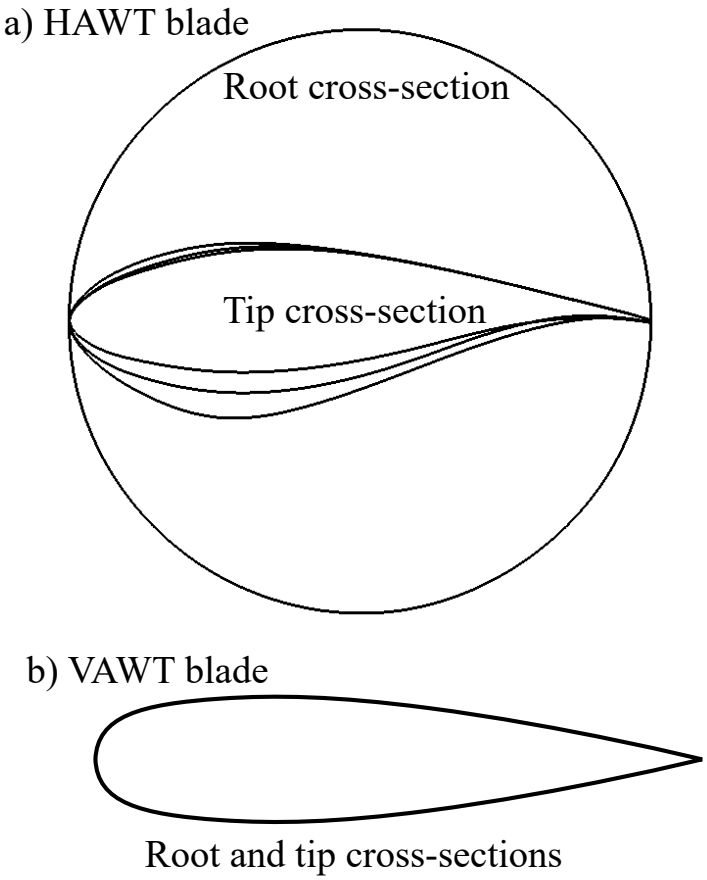

Figure 13. (**a**) Cross-sections of HAWT blade NREL 5 MW and (**b**) cross-sections of VAWT blade with symmetric NACA profile.

In terms of decommissioning of HAWT blades, creative solutions have emerged, for example, the Meidoorn playground in Rotterdam, The Netherlands, or innovative house designs [91].

The recycling of HAWT blades, however, involves a more creative design process for using the root and leading-edges of the blade. Additionally, the blade needs to be cut into unorthodox shapes to accommodate the creative part of the design process. This increases the cost of decommissioning and inevitably, some parts of the blade are left unutilised. In contrast, VAWT blade shapes, both straight and curved, can be re-utilised in a more straight forward manner. For example, in playground parks or as housing material.

Examples of playground and housing for VAWT blade recycling are shown in Figure 14a and Figure 14b, respectively. However, we note that the potential applications are vast and an interesting area to investigate.

a) Playground

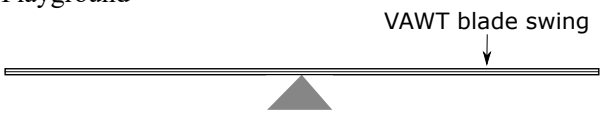

b) Sustainable housing

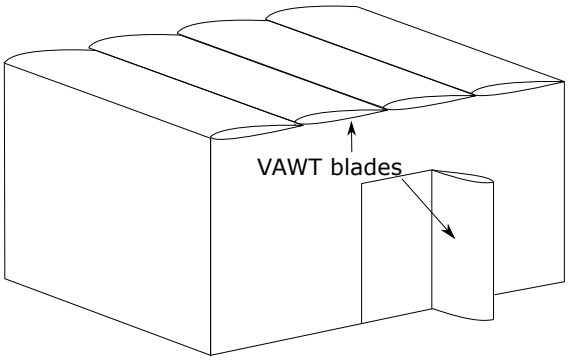

Figure 14. (**a**) VAWT blade—swing (**b**) VAWT blade—roof and door materials.

9. Technology Readiness Level (TRL)

In this section, we compare the technology readiness level (TLR) of large-scale offshore floating HAWTs with offshore floating VATWs.

The reference cases for floating HAWTs are the Hywind Scotland and Hywind Tampen windfarms. Both farms have floating offshore HAWTs rated at 6 MW and 8.8 MW, respectively. In contrast, no reference cases exist for large-scale floating offshore VAWTs. Therefore, the assessment for floating VAWTs is performed based on individual turbine components, lessons learnt and reports published by small-scale developers, and research consortia [9,14,17,19,23,24,92].

In Table 4, we utilise four main categories for the TRL classification: nacelle and hub, blades, tower and full system. Each category is divided into some of the main individual components suggested by the CATAPULT Offshore Renewable Guide [93]. A TRL level is assigned to each component. We follow the TRL scale suggested by the European Marine Energy Centre (EMEC), that varies between 1 to 9, where 9 is technology that is commercially ready [94]. Results of the assessment are shown in Table 4. Two floating HAWTs and two hypothetical large-scale floating VAWTs rated at 5 and 10 MW are considered. The table shows a high TRL level (7–8) for the large-scale floating HAWTs at the individual turbine components, as well as at the full integral system. This is because Hywind Scotland, with turbines rated at 6 MW, is already at an operational level. The TRL level at the individual turbine component of floating VAWTs is ranked at an average value of 6. This is because most of the turbine components have been proven to be operational onshore. We recall, for example, that the largest onshore VAWT ever built was rated at 3.8 MW [14]. The TRL level of some of the subcomponents, however, such as the main bearing, power take-off and control systems, depends on the specific design of the VAWT turbine (variable speed, constant speed, floating axis, etc.) and is ranked accordingly at a TRL level of 3.

The biggest gap between floating offshore HAWTs and VAWTs is identified at the integral level (bottom row of Table 4). This is because large-scale floating VAWTs have not been implemented yet. We note that this trend might change in the near future [22]. Furthermore, rapid progress between TRL levels is nowadays possible given that the individual turbine components and the knowledge, and technology readiness of floating structures is high. With adequate investment and technological innovations, the TRL level of floating VAWTs can be brought to the same level as that of floating HAWTs.

Table 4. TRL assessment of 5 MW and 10 MW floating offshore HAWT and VAWT at subcomponent and at full integral level. The TRL level is ranked between 1 to 9, and N/A is used when the subcategory does not apply to the type of turbine.

Turbine Component	Subcomponent	Floating HAWT		Floating VAWT	
		5 MW	10 MW	5 MW	10 MW
Nacelle and hub	Bed plate	8	7	6	6
	Main bearing	8	7	3	3
	Main shaft	8	7	6	6
	Gearbox	8	7	6	6
	Generator	8	7	6	6
	Power take-off	8	7	3	3
	Control system	8	7	3	3
	Yaw system	8	7	N/A	N/A
	Yaw bearing	8	7	N/A	N/A
	Spinner	8	7	N/A	N/A
Blades	Blades	8	7	6	6
	Blade bearings	8	7	6	6
	Pitch system	8	7	6	6
Tower	Steel	8	7	6	6
	Tower internals	8	7	6	6
Full system	Turbine + floating structure	8	7	3	2

In the next section, we outline a range of innovative technology solutions and delineate potential areas of further research that can help in bridging the gap between large-scale floating VAWTs and HAWTs.

10. Way Forward to Increase TRL

In order to develop the TRL level at integral level and at subcomponent level for floating VAWTs, we have identified some potential avenues of research, which we introduce in the following paragraphs.

Fluid and structure interactions: Although progress has been made towards understanding full system dynamics of two-bladed floating VAWTs [68], much remains unknown in terms of VAWT system dynamics of multi-bladed rotors subject to directional waves and extreme wave loading. Furthermore, turbulent effects in floating VAWTs remain vastly unexplored. It has been stipulated that two-bladed VAWTs could benefit from turbulent fluctuations [34], however, it is not clear which turbulent length scales could be beneficial. HAWT recent studies have shown that turbulence intensity and scale positively affect power generation [95]. Hence this needs to be addressed for floating VAWTs. A better understanding of wave and turbulent effects in floating offshore VAWTs can lead to quantification of these effects in the fatigue life of the turbine. This is of paramount importance in order to design systems that can survive the offshore environment for extended periods of time. Better understanding of wave and floating VAWT interactions can lead to innovative floating structures of variable mass that modify their natural frequencies and avoid resonance. Lastly, it is expected that encounters between gusts and floating VAWTs will alter the performance and dynamics of the turbine. Recent advances in gust and aerofoil encounters [96,97] hint that gust loading on the blade could decrease its fatigue life. However, it remains unknown what the gust influence is in the aerodynamics and system dynamics of a floating VAWT. An improved understanding of these fluid and structure interactions can help in adapting or developing VAWT technology for the floating offshore environment.

Mechanical design: Secondly, cyclic loading of two-bladed VAWTs needs to be addressed. Loading oscillations are of particular concern due to their negative impact in the fatigue life of the structures. Proven solutions to two-bladed VAWT cyclic loading are the use of compliant couplings or the addition of a third blade [31]. More recent solutions are

innovative designs that eliminate the main bearing. For example Salter's multi-bladed ring vertical turbine [98] or Akimoto's floating axis turbine [23,24]. Although Salter's turbine was originally designed as a tidal turbine (see Figure 15), the concept can be adapted to a floating VAWT. The original tidal design is rated to 200 MW, with variable pitch, contra-rotation and power generation from a ring-cam bearing. The turbine is multi-bladed and the blades are supported by two rings at both ends. In contrast, Akimoto's floating axis turbine utilises the axis of the turbine as a spar buoy to sustain the weight of the turbine. The axis of the turbine rotates, and a set of external rollers convert the rotational motion of the shaft to electrical power.

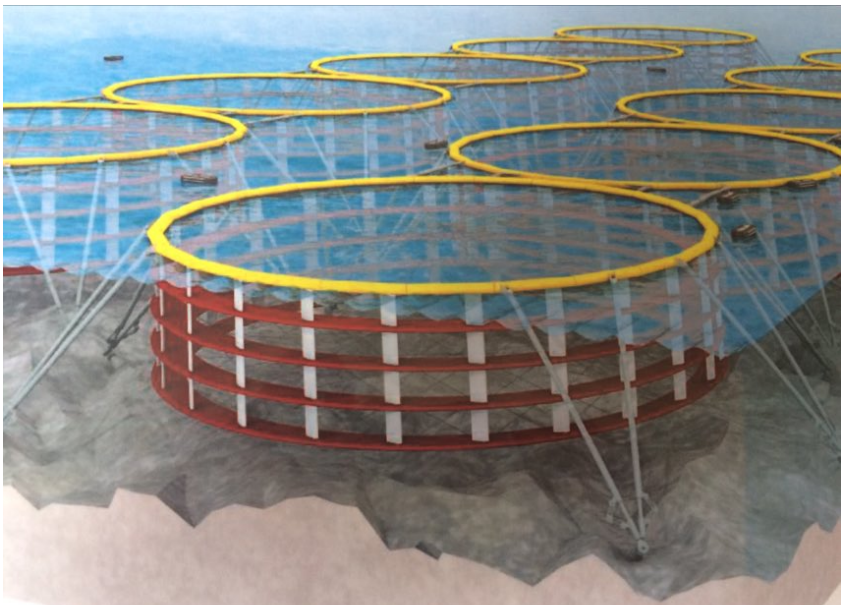

Figure 15. Bearingless vertical axis tidal turbine array by Salter. Source: [99].

Advanced materials: Finally, the use of advanced materials focused on blade morphing and variable stiffness mooring can help in mitigating cyclic loading issues of floating VAWTs. Smart materials that bend in response to external loads have the ability to attenuate the energy absorbed by the structure by means of deformation. This deformation mitigates the change in loads sensed by the blades and therefore prolongs the fatigue life of the turbine. The effectiveness in load alleviation of morphing blades has been recently demonstrated [100–102]. Hence, it is foreseen that flexible material blades can extend the fatigue life of offshore floating VAWTs.

We summarise in Table 5 the areas of research, subcategories and specific topics that we have identified as areas of further research that can help in improving the TRL level of floating VAWTs.

Table 5. Summary of areas of research, subcategories and specific topics to increase the TRL level of offshore floating VAWTs. In the table VAWT refers to floating VAWT.

Area of Research	Subcategory	Specific Topics
Fluid and structure interactions	VAWT turbulence interactions	Turbulence scale and intensity
	VAWT wave interactions	Directional waves, extreme waves
	VAWT gust encounters	Fatigue life, control strategies
Mechanical design	Bearingless solutions	Salter's turbine
		Akimoto's turbine
Advanced materials	Morphing blades	Smart materials
	Variable stiffness moorings	Smart materials

11. Conclusions

Deployment of HAWTs in deep water locations is happening through floating platforms. This, however, poses challenges that have not been encountered before in HAWT development. Maintaining the structural integrity of the turbine, while simultaneously, reducing the levelised cost of energy, becomes increasingly difficult as turbines grow in size. In particular, thrust forces and gravity cyclic loading due to larger blades are of notable concern.

Hence, in this paper, we analyse whether VAWTs could become a feasible alternative for deep water floating arrays and overcome some of the structural and economical challenges associated with large-scale floating turbines. To this aim, a review is performed over different aspects of VAWTs in the context of floating turbines. We highlight some of the opportunities and challenges for floating VAWTs. Different characteristics are assessed: power capture, loading characteristics, stability, type of floating structure, reliability, environment, manufacturing and decommissioning, and technology readiness level (TRL). Some of these aspects are compared to those of floating HAWTs, where appropriate.

Our analysis shows that an increased wind farm power density and an increased reliability could be decisive factors to make VAWTs a feasible alternative for floating arrays. Additionally, circular economy considerations such as ease of manufacturing of the blades and simpler routes to blade recycling, constitute a sustainable framework for VAWT offshore technology. Hence, the authors of this paper believe that VAWTs are a feasible alternative for deep water floating deployments.

It is noted, however, that the TRL level of VAWTs needs to be increased to become a fully viable alternative. Hence, adequate investment and government policies are needed. Industry trends show that a large-scale floating VAWT ($\sim$1 MW) might be in operation in Sweden by 2023 [22]. This is a promising outlook, but further interest from stakeholders across the globe needs to be raised.

Finally, we identify areas of research and development that can help in increasing the TRL level of VAWTs. These are: (1) an increased understanding of wave, turbulent and gust loading interactions, (2) bearingless VAWT solutions and (3) advanced materials with particular application to blade morphing and variable stiffness moorings. Efforts in these areas in conjunction with the advantages that VAWTs already have for floating deployments can transform traditional views and make floating VAWTs a reality for deep water arrays.

Author Contributions: Conceptualization, methodology, experimental tests, investigation, writing original draft, writing review and editing, data curation, A.A.-G.; conceptualization, methodology, investigation, writing review and editing, supervision, project administration, funding acquisition, F.B. All authors have read and agreed to the published version of the manuscript.

Funding: This research was in part funded by Scottish Enterprise.

Institutional Review Board Statement: Not applicable.

Informed Consent Statement: Not applicable.

Data Availability Statement: All data that support the findings of this study are included within the article.

Acknowledgments: The authors acknowledge the input of project partners, NSRI, Subsea UK, Wood Group.

Conflicts of Interest: The authors declare no conflict of interest.

Appendix A

This appendix shows the dimensions of the turbines in clusters A, B and C used to plot Figure 9. Cluster A corresponds to turbines in Figure 3.

Table A1. HAWT turbine specifications.

HAWT Parameter	5 MW	10 MW	15 MW
Hub height (m)	90	113	125
Diameter (m)	126	169	195
Height (m)	153	198	223
Blade length (m)	61.5	83	95
Swept Area (m^2)	12,469	22,444	29,926
Rated wind speed (m/s)	11.4	11.7	12.0
Thrust (N)	5.7×10^5	11×10^5	15×10^5
OTM (Nm)	5.1×10^7	12×10^7	19×10^7

Table A2. Darrieus turbine specifications (Here, blade length is half the circumference of an ellipse with the height provided on the table).

HAWT Parameter	3 MW	8 MW	11 MW
Diameter (m)	101	135	156
Height (m)	161	213	244
Blade length (m)	200	268	309
Swept Area (m^2)	11,970	21,534	28,670
Rated wind speed (m/s)	11.3	11.6	11.8
Thrust (N)	4.3×10^5	8.2×10^5	11×10^5
OTM (Nm)	3.7×10^7	9.1×10^7	14×10^7

Table A3. H-Rotor turbine specifications.

HAWT Parameter	5 MW	10 MW	15 MW
Diameter (m)	126	169	195
Height (m)	136	179	205
Blade length (m)	126	169	195
Swept Area (m^2)	15,589	28,561	38,025
Rated wind speed (m/s)	11.2	11.5	11.6
Thrust (N)	5.5×10^5	1×10^5	14×10^5
OTM (Nm)	4.07×10^7	10×10^7	16×10^7

References

1. Rodrigues, S.; Restrepo, C.; Kontos, E.; Teixeira Pinto, R.; Bauer, P. Trends of offshore wind projects. *Renew. Sustain. Energy Rev.* **2015**, *49*, 1114–1135. [CrossRef]
2. Higgins, P.; Foley, A. The evolution of offshore wind power in the United Kingdom. *Renew. Sustain. Energy Rev.* **2014**, *37*, 599–612. [CrossRef]
3. Policy Paper. Offshore Wind: Sector Deal. Available online: https://www.gov.uk/government/publications/offshore-wind-sector-deal (accessed on 19 August 2021).
4. Press Release. New Plans to Make UK World Leader in Green Energy. Available online: https://www.gov.uk/government/news/new-plans-to-make-uk-world-leader-in-green-energy (accessed on 19 August 2021).
5. Danish Energy Agency. Energy Island in the North Sea. Available online: https://ens.dk/en/our-responsibilities/wind-power/energy-islands/energy-island-north-sea (accessed on 14 July 2021).
6. China's First Floating Wind Turbine Heads Offshore. Available online: https://www.offshorewind.biz/2021/07/13/chinas-first-floating-wind-turbine-heads-offshore/ (accessed on 14 July 2021).
7. V236-15.0 MW at a Glance. Available online: https://www.vestas.com/en/products/offshore-platforms/ (accessed on 14 July 2021).
8. Li, L.; Liu, Y.; Yuan, Z.; Gao, Y. Wind field effect on the power generation and aerodynamic performance of offshore floating wind turbines. *Energy* **2018**, *157*, 379–390. [CrossRef]

9. Griffith, D.T.; Barone, M.F.; Paquette, J.; Owens, B.C.; Bull, D.L.; Simao-Ferriera, C.; Goupee, A.; Fowler, M. *Design Studies for Deep-Water Floating Offshore Vertical Axis Wind Turbines*; Sandia Report; Sandia National Lab. (SNL-NM): Albuquerque, NM, USA, 2018. [CrossRef]
10. Tjiu, W.; Marnoto, T.; Mat, S.; Ruslan, M.H.; Sopian, K. Darrieus vertical axis wind turbine for power generation II: Challenges in HAWT and the opportunity of multi-megawatt Darrieus VAWT development. *Renew. Energy* **2015**, *75*, 560–571. [CrossRef]
11. Eriksson, S.; Bernhoff, H.; Leijon, M. Evaluation of different turbine concepts for wind power. *Renew. Sustain. Energy Rev.* **2008**, *12*, 1419–1434. [CrossRef]
12. Mohan Kumar, P.; Sivalingam, K.; Lim, T.C.; Ramakrishna, S.; Wei, H. Review on the Evolution of Darrieus Vertical Axis Wind Turbine: Large Wind Turbines. *Clean Technol.* **2019**, *1*, 205–223. [CrossRef]
13. Islam, M.; Ting, D.S.K.; Fartaj, A. Aerodynamic models for Darrieus-type straight-bladed vertical axis wind turbines. *Renew. Sustain. Energy Rev.* **2008**, *12*, 1087–1109. [CrossRef]
14. Möllerström, E.; Gipe, P.; Beurskens, J.; Ottermo, F. A historical review of vertical axis wind turbines rated 100 kW and above. *Renew. Sustain. Energy Rev.* **2019**, *105*, 1–13. [CrossRef]
15. 4navitas. Available online: https://www.4navitas.com/ (accessed on 12 June 2021).
16. Swift TG Energy. Available online: http://www.swifttgenergy.com/ (accessed on 13 June 2021).
17. Shires, A. Design optimisation of an offshore vertical axis wind turbine. *Proc. Inst. Civ. Eng.-Energy* **2013**, *166*, 7–18. [CrossRef]
18. Collu, M.; Brennan, F.; Patel, M. Conceptual design of a floating support structure for an offshore vertical axis wind turbine: The lessons learnt. *Ships Offshore Struct.* **2014**, *9*, 3–21. [CrossRef]
19. Paulsen, U.S.; Madsen, H.A.; Kragh, K.A.; Nielsen, P.H.; Baran, I.; Hattel, J.; Ritchie, E.; Leban, K.; Svendsen, H.; Berthelsen, P.A. DeepWind-from Idea to 5 MW Concept. *Energy Procedia* **2014**, *53*, 23–33. [CrossRef]
20. Floating Wind & Current Hybrid Power Generation [Skwíd]. Available online: https://www.cleanenergy-project.de/wp-content/uploads/2013/06/www.modec.com_fps_skwid_pdf_skwid.pdf (accessed on 18 November 2021).
21. Ademe. Vertiwind. Available online: https://www.ademe.fr/sites/default/files/assets/documents/en_vertiwind.pdf (accessed on 12 June 2021).
22. SEATWIRL. The Future of Offshore Wind. Available online: https://seatwirl.com/ (accessed on 13 June 2021).
23. Akimoto, H.; Tanaka, K.; Uzawa, K. Floating axis wind turbines for offshore power generation—A conceptual study. *Environ. Res. Lett.* **2011**, *6*, 044017. [CrossRef]
24. Akimoto, H.; Iijima, K.; Takata, Y. Feasibility Study of the Floating Axis Wind Turbine: Preliminary Model Experiments. In Proceedings of the 36th International Conference on Offshore Mechanics and Arctic Engineering, Trondheim, Norway, 25–30 June 2017. [CrossRef]
25. Hand, B.; Kelly, G.; Cashman, A. Aerodynamic design and performance parameters of a lift-type vertical axis wind turbine: A comprehensive review. *Renew. Sustain. Energy Rev.* **2021**, *139*, 110699. [CrossRef]
26. Burton, T.; Jenkins, N.; Sharpe, D.; Bossanyi, E. *Wind Energy Hand Book*, 2nd ed.; John Wiley & Sons Ltd.: Chichester, UK, 2011.
27. Jonkman, J.; Matha, D. *Quantitative Comparison of the Responses of Three Floating Platforms*; National Renewable Energy Laboratory: Golden, CO, USA, 2010.
28. Marten, D.; Wendler, J.; Pechlivanoglou, G.; Nayeri, C.; Paschereit, C. QBlade: An open source tool for desing and siulation of a horizontal and vertical axis wind turbines. *Int. J. Emerg. Technol. Adv. Eng.* **2013**, *3*, 264–269.
29. Zanon, A.; De Gennaro, M.; Kühnelt, H. Wind energy harnessing of the NREL 5 MW reference wind turbine in icing conditions under different operational strategies. *Renew. Energy* **2018**, *115*, 760–772. [CrossRef]
30. Ashwill, T.D. *Measured Data for the Sandia 34-meter Vertical Axis Wind Turbine*; Td Sandia Natl. Lab.: Albuquerque, NM, USA, 1992.
31. Sutherland, H.J.; Berg, D.E.; Ashwill, T.D. *A Retrospective of VAWT Technology*; Td Sandia Natl. Lab.: Albuquerque, NM, USA; Livermore, CA, USA, 2012.
32. Morgan, C.A.; Gardner, P.; Mays, I.D.; Anderson, M.B. The demonstration of a stall regulated 100 kW vertical axis wind turbine. In Proceedings of the European Wind Energy Conference, Glasgow, Scotland, 10–13 July 1989.
33. Brusca, S.; Lanzafame, R.; Messina, M. Design of a vertical-axis wind turbine: How the aspect ratio affects the turbine's performance. *Int. J. Energy Environ. Eng.* **2014**, *5*, 333–340. [CrossRef]
34. Rezaeiha, A.; Montazeri, H.; Blocken, B. Characterization of aerodynamic performance of vertical axis wind turbines: Impact of operational parameters. *Energy Convers. Manag.* **2018**, *169*, 45–77. [CrossRef]
35. Jonkman, J.; Butterfield, S.; Musial, W.; Scott, G. *Definition of a 5-MW Reference Wind Turbine for Offshore System Development*; National Renewable Energy Laboratory: Golden, CO, USA, 2009. [CrossRef]
36. Schwartz, M.; Heimiller, D.; Haymes, S.; Musial, W. *Assessment of Offshore Wind Energy Resources for the United States*; National Renewable Energy Laboratory: Golden, CO, USA, 2010. [CrossRef]
37. Vorpahl, F.; Schwarze, H.; Fischer, T.; Seidel, M.; Jonkman, J. Offshore wind turbine environment, loads, simulation, and design. *Wires Energy Environ.* **2013**, *2*, 548–570. [CrossRef]
38. Golbazi, M.; Archer, C.L. Surface roughness for offshore wind energy. *J. Phys. Conf. Ser.* **2020**, *1452*, 012024. [CrossRef]
39. Sathe, A.; Bierbooms, W. Influence of different wind profiles due to varying atmospheric stability on the fatigue life of wind turbines. *J. Phys. Conf. Ser.* **2007**, *75*, 012056. [CrossRef]
40. Jung, C.; Schindler, D. The role of the power law exponent in wind energy assessment: A global analysis. *Int. J. Energy Res.* **2021**, *45*, 8484–8496. [CrossRef]

41. Howland, M.F.; González, C.M.; Martínez, J.J.P.; Quesada, J.B.; Larrañaga, F.P.; Yadav, N.K.; Chawla, J.S.; Dabiri, J.O. Influence of atmospheric conditions on the power production of utility-scale wind turbines in yaw misalignment. *J. Renew. Sustain. Energy* **2020**, *12*, 063307. [CrossRef]
42. Verelst, D.R.S.; Larsen, T.J.; van Wingerden, J.W. Wind tunnel tests of a free yawing downwind wind turbine. *J. Phys. Conf. Ser.* **2014**, *555*, 012103. [CrossRef]
43. Geos, F. *Wind and Wave Frequency Distributions for Sites around the British Isles*; Offshore Technology Report; HSE Books: Norwich, UK, 2001.
44. Leithead, W. Wind energy. *Philos. Trans. R. Soc. A Math. Phys. Eng. Sci.* **2007**, *365*, 957–970. [CrossRef] [PubMed]
45. Dao, C.; Kazemtabrizi, B.; Crabtree, C. Wind turbine reliability data review and impacts on levelised cost of energy. *Wind Energy* **2019**, *22*, 1848–1871. [CrossRef]
46. Müller, S.; Muhawenimana, V.; Wilson, C.A.; Ouro, P. Experimental investigation of the wake characteristics behind twin vertical axis turbines. *Energy Convers. Manag.* **2021**, *247*, 114768. [CrossRef]
47. Dabiri, J.O. Potential order-of-magnitude enhancement of wind farm power density via counter-rotating vertical-axis wind turbine arrays. *J. Renew. Sustain. Energy* **2011**, *3*, 043104. [CrossRef]
48. Abkar, M. Theoretical Modeling of Vertical-Axis Wind Turbine Wakes. *Energies* **2019**, *12*, 10. [CrossRef]
49. Ouro, P.; Lazennec, M. Theoretical modelling of the three-dimensional wake of vertical axis turbines. *Flow* **2021**, *1*, E3. [CrossRef]
50. Musial, W. Offshore wind energy facility characteristics. In Proceedings of the BOEM's Offshore Wind and Maritime Industry Knowledge Exchange Workshop, Baltimore, MD, USA, 5–6 March 2018.
51. MacKay, D. *Sustainable Energy—Without the Hot Air*; UIT Cambridge Ltd.: Cambridge, UK, 2008.
52. Templin, R.J. *Aerodynamic Performance Theory for the NRC Vertical-Axis Wind Turbine*; Technical Report LTR-LA-160; National Aeronautical Establishment: Ottawa, ON, Canada, 1974.
53. Strickland, J.H. A performance prediction model for the darrieus turbine. In Proceedings of the International Symposium on Wind Energy Systems, Cambridege, UK, 7–9 September 1976.
54. Paraschivoiu, I. *Double-Multiple Streamtube Model for Darrieus in Turbines*; NASA Lewis Research Center Wind Turbine Dynamics: Cleveland, OH, USA, 1981.
55. Madsen, H.; Larsen, T.; Vita, L.; Paulsen, U. Implementation of the Actuator Cylinder flow model in the HAWC2 code for aeroelastic simulations on Vertical Axis Wind Turbines. In Proceedings of the 51st AIAA Aerospace Sciences Meeting Including the New Horizons Forum and Aerospace Exposition, Grapevine, TX, USA, 7–10 January 2013. [CrossRef]
56. Ning, A. Actuator cylinder theory for multiple vertical axis wind turbines. *Wind Energy Sci.* **2016**, *1*, 327–340. [CrossRef]
57. Meng, F.; Schwarze, H.; Vorpahl, F.; Strobel, M. A free wake vortex lattice model for vertical axis wind turbines: Modeling, verification and validation. *J. Phys. Conf. Ser.* **2014**, *555*, 012072. [CrossRef]
58. Giles, A.D. *Wind Panel Manual: Modelling the Aerodynamics of Wind Turbines*; University of Strathclyde: Glasgow, UK, 2017.
59. Hirsch, I.H.; Mandal, A. A Cascade Theory for the Aerodynamic Performance of Darrieus Wind Turbines. *Wind Eng.* **1987**, *11*, 164–175.
60. Bensason, D.; Fouest, S.L.; Young, A.; Mulleners, K. Greenberg's force prediction for vertical-axis wind turbine blades. *arXiv* **2021**, arXiv:2111.00871.
61. Hansen, J.T.; Mahak, M.; Tzanakis, I. Numerical modelling and optimization of vertical axis wind turbine pairs: A scale up approach. *Renew. Energy* **2021**, *171*, 1371–1381. [CrossRef]
62. Su, J.; Li, Y.; Chen, Y.; Han, Z.; Zhou, D.; Zhao, Y.; Bao, Y. Aerodynamic performance assessment of φ-type vertical axis wind turbine under pitch motion. *Energy* **2021**, *225*, 120202. [CrossRef]
63. Collu, M.; Borg, M.; Shires, A.; Brennan, F.P. FloVAWT: Progress on the Development of a Coupled Model of Dynamics for Floating Offshore Vertical Axis Wind Turbines. In Proceedings of the 32nd International Conference on Offshore Mechanics and Arctic Engineering, Nantes, France, 9–14 June 2013. [CrossRef]
64. Hand, B.; Cashman, A.; Kelly, G. A Low-Order Model for Offshore Floating Vertical Axis Wind Turbine Aerodynamics. *IEEE Trans. Ind. Appl.* **2017**, *53*, 512–520. [CrossRef]
65. Cheng, Z.; Madsen, H.A.; Gao, Z.; Moan, T. A fully coupled method for numerical modeling and dynamic analysis of floating vertical axis wind turbines. *Renew. Energy* **2017**, *107*, 604–619. [CrossRef]
66. LeBlanc, B.P.; Ferreira, C.S. Experimental Determination of Thrust Loading of a 2-Bladed Vertical Axis Wind Turbine. *J. Phys. Conf. Ser.* **2018**, *1037*, 022043. [CrossRef]
67. Delafin, P.L.; Nishino, T.; Wang, L.; Kolios, A. Effect of the number of blades and solidity on the performance of a vertical axis wind turbine. *J. Phys. Conf. Ser.* **2016**, *753*, 022033. [CrossRef]
68. Borg, M.; Collu, M. A comparison between the dynamics of horizontal and vertical axis offshore floating wind turbines. *Philos. Trans. R. Soc. A Math. Phys. Eng. Sci.* **2015**, *373*, 20140076. [CrossRef]
69. Butterfield, S.; Musial, W.; Jonkman, J.; Sclavounos, P. Engineering Challenges for Floating Offshore Wind Turbines. In Proceedings of the Copenhagen Offshore Wind Conference, Copenhagen, Denmark, 26–28 October 2005.
70. Seawind. Available online: https://seawindtechnology.com/ (accessed on 27 June 2021).
71. Laura, C.S.; Vicente, D.C. Life-cycle cost analysis of floating offshore wind farms. *Renew. Energy* **2014**, *66*, 41–48. [CrossRef]
72. Ultra-Deep Water Port: Feasibility Study. Available online: https://www.gov.scot/publications/ultra-deep-water-feasibility-study-report/pages/5/ (accessed on 3 September 2021).

73. Next Step for Hywind Tampen. Available online: https://www.equinor.com/en/news/20210422-next-step-hywind-tampen.html (accessed on 3 September 2021).
74. Tupper, E.C. *Introduction to Naval Architecture*, 5th ed.; Butterworth-Heinemann: Jersey City, NJ, USA, 2013.
75. Martin, R.; Lazakis, I.; Barbouchi, S.; Johanning, L. Sensitivity analysis of offshore wind farm operation and maintenance cost and availability. *Renew. Energy* **2016**, *85*, 1226–1236. [CrossRef]
76. Dinwoodie, I.; McMillan, D.; Quail, F. Analysis of offshore wind turbine operation and maintenance using a novel time domain meteo-ocean modeling approach. In Proceedings of the ASME Turbo Expo 2012: Turbine Technical Conference and Exposition, Copenhagen, Denmark, 11–15 June 2012.
77. Carroll, J.; McDonald, A.; McMillan, D. Failure rate, repair time and unscheduled O&M cost analysis of offshore wind turbines. *Wind Energy* **2016**, *19*, 1107–1119. [CrossRef]
78. Artigao, E.; Martín-Martínez, S.; Honrubia-Escribano, A.; Gómez-Lázaro, E. Wind turbine reliability: A comprehensive review towards effective condition monitoring development. *Appl. Energy* **2018**, *228*, 1569–1583. [CrossRef]
79. Kails, K.; Li, Q.; Mueller, M. A modular and cost-effective high-temperature superconducting generator for large direct-drive wind turbines. *IET Renew. Power Gener.* **2021**, *15*, 2022–2032. [CrossRef]
80. Manning, P.T. The Environmental Impact of the Use of Large Wind Turbines. *Wind Eng.* **1983**, *7*, 1–11.
81. Drewitt, A.L.; Langston, R.H.W. Assessing the impacts of wind farms on birds. *Ibis* **2006**, *148*, 29–42. [CrossRef]
82. Islam, M.; Mekhilef, S.; Saidur, R. Progress and recent trends of wind energy technology. *Renew. Sustain. Energy Rev.* **2013**, *21*, 456–468. [CrossRef]
83. Dabiri, J.O.; Greer, J.R.; Koseff, J.R.; Moin, P.; Peng, J. A new approach to wind energy: Opportunities and challenges. *AIP Conf. Proc.* **2015**, *1652*, 51–57. [CrossRef]
84. Santangeli, A.; Katzner, T. A call for conservation scientists to evaluate opportunities and risks from operation of vertical axis wind turbines. *Front. Ecol. Evol.* **2015**, *3*, 68. [CrossRef]
85. Hüppop, O.; Dierschke, J.; Exo, K.M.; Fredrich, E.; Hill, R. Bird migration studies and potential collision risk with offshore wind turbines. *Ibis* **2006**, *148*, 90–109. [CrossRef]
86. Marques, A.T.; Batalha, H.; Rodrigues, S.; Costa, H.; Pereira, M.J.R.; Fonseca, C.; Mascarenhas, M.; Bernardino, J. Understanding bird collisions at wind farms: An updated review on the causes and possible mitigation strategies. *Biol. Conserv.* **2014**, *179*, 40–52. [CrossRef]
87. Wang, S.; Wang, S.; Smith, P. Ecological impacts of wind farms on birds: Questions, hypotheses, and research needs. *Renew. Sustain. Energy Rev.* **2015**, *44*, 599–607. [CrossRef]
88. Tomaszewski, J.M.; Lundquist, J.K.; Churchfield, M.J.; Moriarty, P.J. Do wind turbines pose roll hazards to light aircraft? *Wind Energy Sci.* **2018**, *3*, 833–843. [CrossRef]
89. Howell, R.; Qin, N.; Edwards, J.; Durrani, N. Wind tunnel and numerical study of a small vertical axis wind turbine. *Renew. Energy* **2010**, *35*, 412–422. [CrossRef]
90. ACT Blade: The Lightest and Most Controllable Wind Turbine Blade. Available online: https://www.innoenergy.com/discover-innovative-solutions/product-portfolio/act-blade/ (accessed on 24 May 2021).
91. Bank, L.C.; Arias, F.R.; Yazdanbakhsh, A.; Gentry, T.R.; Al-Haddad, T.; Chen, J.F.; Morrow, R. Concepts for Reusing Composite Materials from Decommissioned Wind Turbine Blades in Affordable Housing. *Recycling* **2018**, *3*, 3. [CrossRef]
92. Blonk, D.L. Conceptual Design and Evaluation of Economic Feasibility of Floating Vertical Axis Wind Turbines. Master's Thesis, TU Delft, Delft, The Netherlands, 2010.
93. CATAPULT. Offshore Renewable Energy. Interactive Guide. Available online: https://guidetoanoffshorewindfarm.com/guide (accessed on 16 July 2021).
94. EMEC. The European Marine Energy Centre LTD. Available online: http://www.emec.org.uk/services/pathway-to-emec/technology-readiness-levels/ (accessed on 16 July 2021).
95. Gambuzza, S.; Ganapathisubramani, B. The effects of free-stream turbulence on the performance of a model wind turbine. *J. Renew. Sustain. Energy* **2021**, *13*, 023304. [CrossRef]
96. Young, A.M.; Smyth, A.S.M. Gust–Airfoil Coupling with a Loaded Airfoil. *AIAA J.* **2021**, *59*, 773–785. [CrossRef]
97. Jones, A.R.; Cetiner, O.; Smith, M.J. Physics and Modeling of Large Flow Disturbances: Discrete Gust Encounters for Modern Air Vehicles. *Annu. Rev. Fluid Mech.* **2022**, *54*, 469–493. [CrossRef]
98. Salter, S.H.; Taylor, J.R.M. Vertical-axis tidal-current generators and the Pentland Firth. *Proc. Inst. Mech. Eng. Part A J. Power Energy* **2007**, *221*, 181–199. [CrossRef]
99. Zhao, R.; Creech, A.C.W.; Borthwick, A.G.L.; Venugopal, V.; Nishino, T. Aerodynamic Analysis of a Two-Bladed Vertical-Axis Wind Turbine Using a Coupled Unsteady RANS and Actuator Line Model. *Energies* **2020**, *13*, 776. [CrossRef]
100. Arredondo-Galeana, A.; Young, A.M.; Smyth, A.S.; Viola, I.M. Unsteady load mitigation through a passive trailing-edge flap. *J. Fluids Struct.* **2021**, *106*, 103352. [CrossRef]
101. Hoerner, S.; Abbaszadeh, S.; Cleynen, O.; Bonamy, C.; Maître, T.; Thévenin, D. Passive flow control mechanisms with bioinspired flexible blades in cross-flow tidal turbines. *Exp. Fluids* **2021**, *62*, 104. [CrossRef]
102. Pisetta, G.; Le Mestre, R.; Viola, I.M. Morphing blades for tidal turbines: A theoretical study. *Renew. Energy* **2021**, in press. [CrossRef]